

Surface Photochemistry of Rh(CO)₂ on Zeolite Y—Production of a Stable Coordinatively Unsaturated Rhodium Monocarbonyl Surface Species at Room Temperature

Xianlong Wang and Edward A. Wovchko*

Department of Chemistry, Bryn Mawr College, 101 North Merion Avenue, Bryn Mawr, Pennsylvania 19010

Received: May 28, 2004; In Final Form: June 29, 2005

The photochemical production and chemical reactivity of a new coordinatively unsaturated rhodium monocarbonyl species on the surface of dealuminated zeolite Y over a temperature range of 300–420 K and a pressure range from 10^{−5} to 20 Torr has been studied. Using high vacuum techniques and transmission infrared spectroscopy, ultraviolet irradiation (350 ± 50 nm) of supported Rh(CO)₂ surface species led to the production of stable, but reactive, =Rh(CO) surface species, characterized by an infrared band at 2023 cm^{−1}. The coordinatively unsaturated =Rh(CO) species convert to less reactive and coordinatively saturated ≡Rh(CO) by thermal treatment above 370 K. The ≡Rh(CO) species were characterized by an infrared band at 2013 cm^{−1}. An explanation of the mode of bonding of the rhodium monocarbonyl species to the zeolite surface is provided. Coordinatively unsaturated =Rh(CO) species captured N₂, H₂, and O₂ gas molecules near room temperature to produce a variety of mixed ligand rhodium surface complexes of the form Rh(CO)(N₂), Rh(CO)(H₂), Rh(CO)(H)₂, Rh(CO)(H), Rh(CO)(O), and Rh(O). Infrared band assignments for the new species are provided. The work provides new insight into the photochemical behavior of Rh(CO)₂ species supported on high-area zeolite materials and may improve our understanding of the role of active rhodium monocarbonyl species in the development of heterogeneous photocatalysts.

1. Introduction

Coordinatively unsaturated rhodium monocarbonyl, Rh(CO), surface species supported on alumina has been shown to be able to activate the C–H bond in alkanes,^{1–5} the H–H bond in H₂,^{5,6} the O=O bond in O₂,^{5,7} and the C=O bond in CO₂ molecules.^{5,8} Similar Rh centers were found in the homogeneous phase to be capable of activating C–H bonds in alkanes,^{9–16} and Si–H bonds in silanes.^{10,14,15} Rhodium monocarbonyl species can be produced by ultraviolet photolysis of Rh(CO)₂ on alumina, or analogous rhodium *gem*-dicarbonyl compounds in solution.^{5,9,10,14,15,17,18} Irradiation causes the loss of a CO ligand to produce a proposed 16-electron intermediate. However, this intermediate could not exist as a stable species for very long on the support nor in homogeneous phase because of its high reactivity. On the alumina support, the coordinatively unsaturated rhodium monocarbonyl species can migrate and react with nearby Rh(CO)₂ surface species to form a stable dinuclear Rh₂-(CO)₃ surface species. Wong and Yates³ found this to be an undesired side reaction during bond activation experiments. In the homogeneous phase, solvent molecules, such as krypton and hexane, usually occupy the vacant site.^{9,11,14} However, analogous dinuclear species may also form.¹⁴

In an effort to generate stable, coordinatively unsaturated rhodium monocarbonyl surface species, zeolite may be a good support material for Rh(CO)₂. Zeolite has a three-dimensional framework structure composed of connected SiO₄ and AlO₄ tetrahedral units.^{19,20} There are regularly distributed cages and pores of different but uniform size. The high surface area of this material is mainly from the inner surface of zeolite, with only a small percentage from the outer surface. Due to the excess

negative charge on Al relative to Si, zeolite surfaces have sites that cations may bind with. The number of available cation sites depends on the Si/Al ratio of the zeolite. Rhodium ions can be incorporated to these cation sites through ion exchange or other methods. Miessner et al.^{21–23} has reported that dealuminated zeolite Y, which has a very high Si/Al ratio with 7.4 Å diameter supercages, supports Rh(CO)₂ species. Strong and very sharp ($\nu_{1/2} \leq 5$ cm^{−1}) antisymmetric and symmetric CO stretching modes from Rh(CO)₂/zeolite appear in the transmission infrared spectrum. The study showed that, in the absence of water and other cations in the zeolite micropores, the Rh complexes remain isolated from each other, as in a matrix, and are unable to interact with each other. All of the Rh(CO)₂ surface species experience a similar chemical environment when on the zeolite inner surface. Provided that the migration energy barrier for rhodium is high and that only one rhodium occupies each supercage, we expect that coordinatively unsaturated rhodium monocarbonyl surface species, produced during photochemical degradation of Rh(CO)₂, could exist for extended periods of time on the inner surface of zeolite.

Using infrared spectroscopy and high vacuum techniques, we have prepared and identified coordinatively unsaturated rhodium monocarbonyl surface species on the surface of dealuminated zeolite Y (CBV600) by UV photolysis of supported Rh(CO)₂. Unlike Rh(CO) species on an alumina support, this active intermediate is stable at room temperature under vacuum. This zeolite-supported coordinatively unsaturated species can reversibly bind N₂ molecules. H₂ and O₂ molecules also bind with rhodium monocarbonyl. Furthermore, the H–H bond and O=O bond were activated. When the temperature of the sample was warmed beyond 370 K, this monocarbonyl species overcame the energy barrier to further react with the zeolite surface to produce very stable, coordinatively saturated rhodium mono-

* Current address of corresponding author: Department of Chemistry, West Virginia Wesleyan College, 59 College Avenue, Buckhannon, WV 26201.

carbonyl species. This stable surface species was inert to N₂ gas molecules tested.

2. Experimental Section

Experiments were conducted in a special, wide temperature range, transmission infrared cell similar in design to that described in detail previously.²⁴ The cell is a stainless steel cube with six conflat flange ports. KBr windows, sealed with differentially pumped double O-rings, were used on two ports for infrared beam transmission. A UV-grade quartz window was used for ultraviolet irradiation. Powdered samples were pressed, under 1200 psi pressure for 30 s, into the closely spaced square openings (0.048 mm²) of a thin tungsten grid (0.025 mm), using a hydraulic press. Excess sample was scraped from the grid using a stainless steel blade. The net mass of deposited samples was 3–4 mg, having an effective surface density in the optical path of 2.0–2.7 mg cm⁻².

The powdered grid was rigidly secured by nickel clamps and attached to electrical feedthroughs mounted on the bottom of a reentrant Dewar that enters the cell. The grid and sample temperature were varied by cooling with Dewar-filled liquid nitrogen or an ethanol/dry ice mixture and by electrical heating with a dc power supply, regulated by a LabView-based digital temperature control program. A chromel/alumel thermocouple (0.08 mm diameter) was spot-welded to the top center of the grid to measure the sample temperature. The temperature could be held constant and maintained to ± 1 K in the range from 100 to 500 K in these experiments. The cell was connected via stainless steel bellows tubing to a Pyrex high vacuum and gas delivery system. The system was pumped by a three-stage oil diffusion pump and backed by a mechanical pump. Prior to experiments, base pressures of 1×10^{-6} Torr, as measured with a cold cathode gauge, were achieved after approximately 12 h of baking. The system was equipped with a KJLC RGA 100F quadrupole mass spectrometer for gas analysis and leak checking. Gas pressures were measured with 0–1 and 0–1000 Torr MKS 626A Baratron capacitance manometers.

Transmission IR spectra of the samples were collected using a pure nitrogen gas purged Nicolet Nexus 470 FT-IR spectrometer equipped with a liquid nitrogen cooled HgCdTe wide band detector. It was controlled by E.Z. Omnic E.S.P. 5.2 software. Spectra were measured at 1-cm⁻¹ resolution in the range from 400 to 4500 cm⁻¹. To optimize the signal-to-noise ratio, 500 scans were averaged per spectrum. Background spectra were measured by translating the cell laterally so the IR beam could pass through a portion of the grid where no sample was deposited. Absorbance spectra of the sample were obtained by ratioing single beam spectra of the sample to background single beam spectra. Spectra have been further processed using OriginLab Origin graphing software.

A 500-W xenon/mercury arc lamp (Oriol Instruments, Stratford, CT) provided ultraviolet light for photolysis experiments. The optical bench was equipped with an f/1 two-element UV-fused silica condensing lens, an iris diaphragm, and a shutter. The light was filtered by a 10-cm water infrared radiation filter and a 3.8 ± 0.5 eV (350 ± 50 nm) band-pass filter (Model 59800, Oriol). Photochemistry and infrared measurements could be conducted simultaneously without disturbing the position of the cell or UV lamp. This was done by orienting the UV light source perpendicular to the infrared beam and the UV light was focused at a 45° angle to the normal of the grid.

The carbon monoxide (Matheson, 99.998%) and oxygen (Matheson, 99.998%) were extracted from lecture bottles and used without further purification. Hydrogen (Airgas, 99.9995%)

was obtained in a steel cylinder and was used without further purification. Nitrogen (Airgas, >99%) was extracted from a steel cylinder and was purified by trapping with liquid N₂. Deuterium (Cambridge, 99.8% D) was obtained in a lecture bottle and used without further purification. Isotopically labeled ¹³C¹⁶O (Icon, 99% ¹³C, 10–12% ¹⁸O) was obtained in a glass breakseal flask and used without further purification.

The 0.5% Rh/zeolite samples were prepared by dissolving RhCl₃·xH₂O (Johnson Matthey, 99.9%) in distilled water. The solution was mixed with the appropriate amount of powered zeolite CBV 600 (Zeolyst, Valley Forge, PA; surface area, 608 m²/g) and ultrasonically dispersed for approximately 30 min. This slurry was mixed with acetone (Aldrich, 99.5%) (9/1 acetone/water volume ratio) and sprayed onto a warmed (~330 K) china dish with a nitrogen gas pressured atomizer. The spraying was interrupted intermediately to allow for solvent evaporation. When finished spraying, the sample was left to dry for about 1 h before transferring to a vial with a stainless steel blade.

Fresh sample was pressed on the grid. The grid/sample assembly was evacuated in the infrared cell and activated at 475 K for about 8 h. Following evacuation, the sample was reduced at 475 K with three 200-Torr H₂ exposures at 10 min each, followed by one 200-Torr H₂ exposure at 60 min duration and evacuation after each exposure. The sample was evacuated and cooled to 292 K and exposed to 10 Torr of CO gas. Then the sample was heated to 400 K for 15 min before the sample was cooled and CO gas was evacuated. Sample spectra were measured at 292 K, except at a different temperature, as indicated.

3. Results

3.1. Formation of Rhodium *gem*-Dicarbonyl Species on Zeolite Y. Initially, well-defined Rh dicarbonyl surface species were prepared in the supercages of the zeolite, which served as the starting material for the subsequent surface chemistry experiments. Rh loadings of 0.5% by mass on zeolite were made through an ion-exchange method. Samples were activated at 475 K for 8 h and then reduced in hydrogen gas at 475 K. Reduced rhodium was expected to exist on both outer and inner surfaces of the zeolite material. By introducing 15 Torr of CO gas into the cell at 300 K, metallic rhodium adsorbed CO to form carbonyl species. At room temperature, metallic carbonyl species slowly converted to isolated Rh(CO)₂ surface species. By heating the samples at 400 K in CO gas, the conversion into isolated Rh(CO)₂ species occurred rapidly and more completely. Characteristic infrared absorption bands at 2118 and 2053 cm⁻¹, due to the antisymmetric and symmetric stretching vibrational modes of Rh(CO)₂, respectively, were readily detected.^{21,23} These bands can be seen in spectrum a of Figure 1. The Rh(CO)₂ spectrum is very similar to the zeolite-supported Rh(CO)₂ infrared spectra obtained in the work of Miessner,^{21,23} indicating similar zeolite chemical environments for rhodium centers. The subtle broadening and shoulder features near the base of the two major features are due to Rh(CO)₂ species anchored at different zeolite cation surface sites and will be the subject of a subsequent publication.²⁵

Though thought to serve as an oxidizing agent and to play a role in the conversion process, surface hydroxyl group infrared band analysis revealed no apparent change during our preparation procedure. Rhodium dicarbonyl species were thermally stable at room temperature. Under vacuum, the intensity of rhodium dicarbonyl bands began to decrease when samples were heated above 500 K. No new infrared bands appeared during thermal decomposition of Rh(CO)₂.

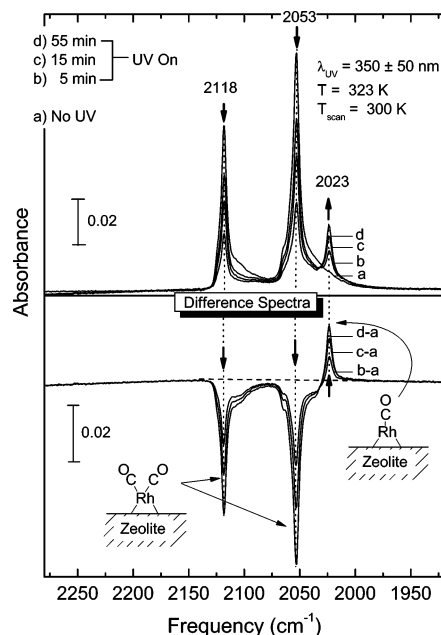


Figure 1. Selected infrared spectra measured in the CO stretching region during 55 min of UV (350 ± 50 nm) photolysis of Rh(CO)₂ supported on zeolite Y (CBV600). The arrows indicate the direction of the absorbance changes. The lower portion presents difference spectra where spectrum a (before UV irradiation) has been subtracted.

3.2. Ultraviolet Photolysis of Rh(CO)₂/Zeolite and Thermal Treatment. The upper portion of Figure 1 shows infrared absorbance spectra measured during the photochemical decomposition of a freshly prepared Rh(CO)₂/zeolite sample at 323 K with 350 ± 50 nm ultraviolet light under vacuum. Spectra b–d are selected infrared spectra of the sample in the carbonyl stretching region at various photolysis times. The lower portion of Figure 1 shows infrared difference spectra, where the spectrum prior to UV light exposure (spectrum a) has been subtracted. The intensity of the Rh(CO)₂ antisymmetric and symmetric stretching bands at 2118 and 2053 cm⁻¹ decreased with the UV irradiation time. A new band at 2023 cm⁻¹ developed with increased UV irradiation time. This band was never observed during Rh(CO)₂ thermal decomposition experiments. There were no other obvious changes in our infrared spectra. Furthermore, the 2023-cm⁻¹ feature did not form when photolyzing Rh(CO)₂/zeolite in the presence of CO gas.

To determine whether the new 2023-cm⁻¹ feature was due to the formation of a new rhodium carbonyl surface species, a photolysis experiment with isotopically labeled rhodium dicarbonyl species was conducted. Infrared spectra of zeolite-supported Rh(¹³C¹⁶O)₂ species, prepared by exposing a freshly reduced sample to 15 Torr of ¹³C¹⁶O gas for 20 min at 400 K, are presented in Figure 2. The antisymmetric and symmetric stretching modes of Rh(¹³C¹⁶O)₂ occurred at 2068 and 2006 cm⁻¹, respectively.^{21,23} Due to ~10% ¹³C¹⁸O and ~1% ¹²C¹⁶O impurities in the ¹³C¹⁶O gas, appreciable amounts of Rh(¹³C¹⁶O)-(¹³C¹⁸O), Rh(¹³C¹⁸O)₂, and Rh(¹²C¹⁶O) (¹³C¹⁶O) isotopomers formed. The infrared band assignments are provided in Figure 2 and in Table 1.

After irradiating the isotopically labeled sample for 20 min with UV light (spectrum b of Figure 2), two new infrared features developed in the carbonyl region at 1977 and 1931 cm⁻¹. The difference spectrum shown in the lower portion of Figure 2 (spectrum b–a) reveals these two bands more clearly. The observed shift to lower frequencies, compared to the new 2023-cm⁻¹ band in Figure 1, indicates that the bands originated from surface carbonyl species. In both the isotopically labeled

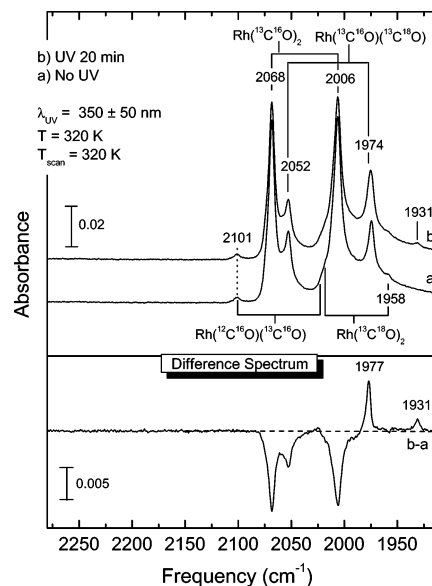


Figure 2. Infrared spectra measured in CO stretching region before (a) and after (b) UV (350 ± 50 nm) irradiation of Rh(¹³CO)₂ supported on zeolite Y (CBV600) for 20 min. The lower portion presents the difference spectrum. Spectra have been offset.

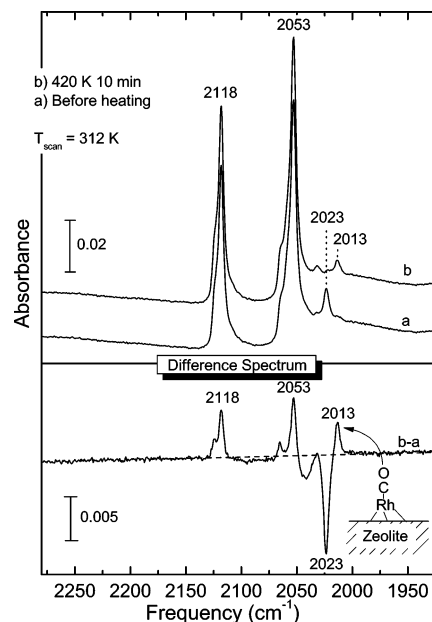


Figure 3. Thermal conversion of coordinatively unsaturated surface species, =Rh(CO), to saturated surface species, =Rh(CO). Infrared spectra measured in CO stretching region before (a) and after (b) heating sample to 420 K for 10 min are shown in the upper portion. The lower portion presents the difference spectrum. Spectra have been offset.

and unlabeled experiments, the intensity of new carbonyl infrared features persisted without change under vacuum up to a thermal treatment temperature of 370 K.

By heating a previously photolyzed Rh(CO)₂/zeolite to 420 K for 10 min under vacuum, additional changes occur in the carbonyl infrared stretching region, as shown in Figure 3. Depletion of the photogenerated band at 2023 cm⁻¹ occurs and a new weak carbonyl feature appears at 2013 cm⁻¹.

3.3. Reversible Reaction of Photogenerated Rh Carbonyl Species with N₂ Gas. The new photochemically produced rhodium carbonyl surface species were reactive to N₂ gas. Spectrum a of Figure 4 shows an infrared absorbance spectrum measured after 20 min UV irradiation of Rh(CO)₂/zeolite at 312 K under vacuum. The prominent 2023-cm⁻¹ band exists. After

TABLE 1: Peak Assignments of Rhodium Carbonyl Species and Other Surface Complexes on Zeolite Y

species	infrared frequency (cm ⁻¹)	reference
Rh(¹² C ¹⁶ O) ₂	$\nu_{as}(\text{CO})$, 2118	$\nu_s(\text{CO})$, 2053
Rh(¹² C ¹⁶ O)(¹³ C ¹⁶ O)	$\nu_{as}(\text{CO})$, 2101	$\nu_s(\text{CO})$, 2021
Rh(¹³ C ¹⁶ O) ₂	$\nu_{as}(\text{CO})$, 2068	$\nu_s(\text{CO})$, 2006
Rh(¹³ C ¹⁶ O)(¹³ C ¹⁸ O)	$\nu_{as}(\text{CO})$, 2052	$\nu_s(\text{CO})$, 1974
Rh(¹³ C ¹⁸ O) ₂	$\nu_{as}(\text{CO})$, 2019	$\nu_s(\text{CO})$, 1958
=Rh(¹² C ¹⁶ O), unsaturated	$\nu(\text{CO})$, 2023	this work
=Rh(¹³ C ¹⁶ O), unsaturated	$\nu(\text{CO})$, 1977	this work
=Rh(¹³ C ¹⁸ O), unsaturated	$\nu(\text{CO})$, 1931	this work
=Rh(¹² C ¹⁶ O), saturated	$\nu(\text{CO})$, 2013	22,23, this work
Rh(¹² C ¹⁶ O)(N ₂)	$\nu(\text{CO})$, 2062	$\nu(\text{N}_2)$, 2252
Rh(¹³ C ¹⁶ O)(N ₂)	$\nu(\text{CO})$, 2027	$\nu(\text{N}_2)$, 2252
Rh(¹³ C ¹⁸ O)(N ₂)	$\nu(\text{CO})$, 1965	$\nu(\text{N}_2)$, 2252
Rh(¹² C ¹⁶ O)(H ₂)	$\nu(\text{CO})$, 2096, 2092	22,23, this work
Rh(¹³ C ¹⁶ O)(H ₂)	$\nu(\text{CO})$, 2047, 2043	23, this work
Rh(¹² C ¹⁶ O)(H) _x , (x = 1,2)	$\nu(\text{CO})$, 2102	this work
Rh(¹² C ¹⁶ O)(D) ₂	$\nu(\text{CO})$, 2098, 2092	this work
Rh(¹² C ¹⁶ O)(D) _x , (x = 1,2)	$\nu(\text{CO})$, 2101	this work

introducing 10 Torr of N₂ gas into the cell, notice that the 2023-cm⁻¹ carbonyl feature disappeared, and new bands formed at 2252 and 2062 cm⁻¹ (spectrum b). The new band at 2252 cm⁻¹ is located in the dinitrogen stretching region and is assigned to a N₂-containing Rh surface species. Difference spectrum b-a in the lower portion of Figure 4 clearly shows the 2062-cm⁻¹ shoulder that developed in the CO stretching region. Upon warming the sample to 370 K in N₂ gas for 1 min, both the 2252-cm⁻¹ N₂ feature and the 2062-cm⁻¹ CO feature diminished in intensity (spectra c and c-b). A weak feature emerged at 2013 cm⁻¹, similar in line shape and intensity to that observed during the thermal treatments displayed in Figure 3. Evidently, slight regeneration of Rh(CO)₂ species also occurred as the 2118- and 2053-cm⁻¹ features grew in intensity.

To demonstrate reversibility in the N₂ adsorption process, Figure 4 includes selected infrared spectra measured from a continuation of the experiment. Spectrum d was recorded after

evacuation of the N₂ gas at 312 K. One may observe further loss of the 2252-cm⁻¹ feature and some regeneration of the original 2023-cm⁻¹ rhodium carbonyl band. The sample was irradiated with UV light for 10 min to regenerate more of the 2023-cm⁻¹ feature (spectrum e). The sample, after reintroduction of 10 Torr of N₂ gas to the cell, exhibited comparable spectroscopic behavior to the first N₂ gas exposure (spectrum f). The surface dinitrogen infrared band at 2252 cm⁻¹ grew while the surface carbonyl band at 2023 cm⁻¹ decreased. The intensity of the weak 2013-cm⁻¹ carbonyl feature did not change appreciably, suggesting chemical inertness of the responsible surface species to N₂.

3.4. Reaction of Photogenerated Rh Carbonyl Species with H₂ and D₂ Gas. Figure 5 contains selected infrared spectra recorded during the reaction of a photolyzed Rh(CO)₂/zeolite sample with H₂ gas at 312 K. Spectrum a reveals a prominent 2023-cm⁻¹ rhodium carbonyl band, produced from UV irradiation. After admitting 20 Torr of H₂ into the cell, the 2023-cm⁻¹ band disappeared immediately (spectrum b). Concurrently, a poorly resolved set of three bands between the antisymmetric and symmetric stretching bands of Rh(CO)₂ emerged. Careful

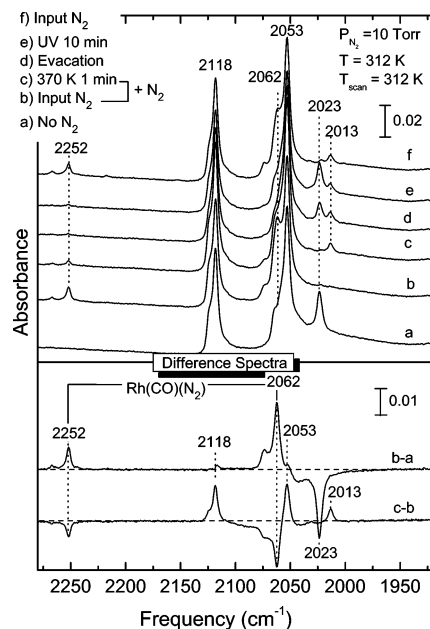


Figure 4. Thermal reaction between 10 Torr of N₂ and coordinatively unsaturated surface species at 312 K. Infrared absorbance spectra measured during the following events are presented in the upper portion. The sample with photochemically generated =Rh(CO) (a) was first exposed to 10 Torr of N₂ (b), followed by flash heating to 370 K (c). Then N₂ gas was evacuated (d) at 312 K, and another 10 min of UV light (350 ± 50 nm) was applied to the sample (e). Finally, another 10 Torr of N₂ was added to the cell (f). The lower portion includes selected difference spectra. Spectra have been offset.

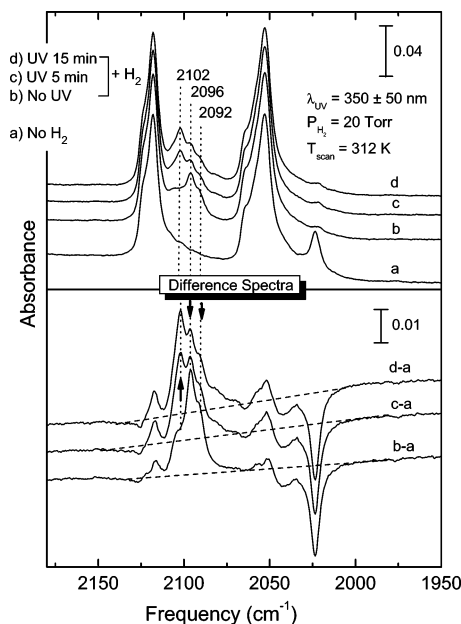


Figure 5. Reaction between 20 Torr of H₂ and coordinatively unsaturated surface species at 312 K. Infrared spectra b-d were recorded in the presence of H₂ gas. Spectra c and d were taken after UV irradiation for the indicated time. The lower portion presents the difference spectra. Spectra have been offset.

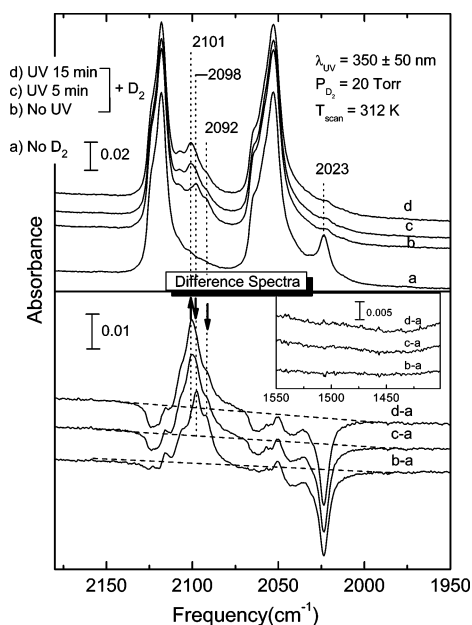


Figure 6. Similar experiment to that conducted in Figure 5. D₂ gas was used. The lower portion presents the difference spectra. The inset in the lower portion shows infrared difference spectra measured in the Rh–D stretching region. Spectra have been offset.

observation and a second derivative of the spectrum indicated band frequencies of 2102, 2096, and 2092 cm⁻¹ for the three overlapping bands. The bands lie in the C–O stretching frequency region^{6,21,23,26} but also in the Rh–H stretching region.²⁷ By exposing the sample to UV light for 5 and 15 min in the presence of H₂ gas, the intensity of 2096- and 2092-cm⁻¹ bands decreased (spectra c and d). Notice on the infrared difference spectra in the lower portion of Figure 5 that the higher frequency 2102-cm⁻¹ band increased significantly during this process. Upon evacuation of H₂ gas from the cell, the bands at 2096 and 2092 cm⁻¹ decreased slightly in intensity. This change resulted in an increase of the Rh(CO)₂ antisymmetric and symmetric stretching mode at 2118 and 2053 cm⁻¹. There was no development at 2023 cm⁻¹.

To further investigate the nature of the new infrared spectroscopic features detected in the H₂ reaction, a reaction was conducted between 20 Torr of D₂ gas and a photolyzed Rh(CO)₂/zeolite sample. Infrared spectra recorded during the reaction are shown in Figure 6. Results, very similar to those in the H₂ reaction, were obtained with D₂. Three overlapping bands develop at 2101, 2098, and 2092 cm⁻¹ in the C–O/Rh–H stretching region. If the bands detected in the D₂ experiment were due to any Rh–D species stretching vibrations, new bands would develop in the 1550–1400-cm⁻¹ region.²⁷ The inset in the lower portion of Figure 6, displaying infrared difference spectra in this region, do not reveal any discernible features. This indicates that the three bands that developed at 2101, 2098, and 2092 cm⁻¹ are due to surface C–O vibrational modes. Furthermore, the line shapes and frequencies of these three overlapping bands from the D₂ experiment (Figure 6, difference spectra) differ slightly from the line shapes and frequencies of the three overlapping bands from the H₂ experiment (Figure 5, difference spectra). There were no other important infrared feature changes except bands forming at 2754, 2677, and 2631 cm⁻¹ due to isotopically labeled isolated surface OD hydroxyl groups and a broad band due to associated surface OD.²⁸

3.5. Reaction of Photogenerated Rh Carbonyl Species with O₂ Gas. Selected infrared difference spectra measured during the reaction between a photolyzed Rh(CO)₂/zeolite sample and

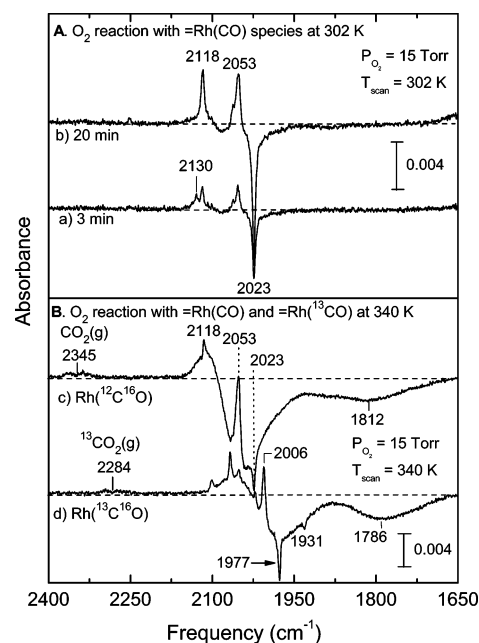


Figure 7. Difference spectra obtained during the O₂ reaction with =Rh(CO). Reactions in section A were conducted at 302 K, while those in section B were conducted at 340 K. Spectra a and b were taken in the presence of 15 Torr of O₂ gas at 302 K in the course of a 20-min reaction. Spectrum c was recorded in the presence of 15 Torr of O₂ at 340 K after a 3-min reaction with =Rh(CO) species. Spectrum d was recorded in the presence of 15 Torr of O₂ gas at 340 K after a 3-min reaction with isotopically labeled =Rh(¹³CO) species.

O₂ gas at 302 K are presented in Figure 7A. Note that the spectrum recorded prior to O₂ exposure has been subtracted. After a 20-min reaction, Rh(CO)₂ bands at 2118 and 2053 cm⁻¹ develop (spectra b). More importantly, a decrease in the 2023-cm⁻¹ rhodium carbonyl band is observed, indicating that a reaction takes place between the rhodium carbonyl species and O₂. After a 3-min reaction, a weak, but distinguishable feature at 2130 cm⁻¹ was detected (spectrum a). This feature lies in the oxidized rhodium carbonyl region.⁷

At 340 K, a CO oxidation reaction was expected to occur between supported rhodium carbonyl species and oxygen. Difference spectrum c in Figure 7B was measured after a 340 K reaction between photolyzed Rh(CO)₂/zeolite and 15 Torr of O₂ gas for 3 min. The 2023-cm⁻¹ rhodium carbonyl band decreased along with a development of an oxidized rhodium carbonyl species infrared band near 2130 cm⁻¹. Unlike the reaction at 302 K, an infrared band centered at 2345 cm⁻¹ was detected in the 340 K reaction, indicating the production of CO₂ gas.²⁹ To confirm this assignment, a 340 K reaction was conducted between O₂ gas and photolyzed Rh(¹³CO)₂/zeolite. Infrared difference spectrum d reveals an appropriately shifted infrared band at 2284 cm⁻¹ due to ¹³CO₂ gas production.²⁹ The broad negative features at 1812 and 1786 cm⁻¹ represent a loss of metallic rhodium carbonyl species still existing on the zeolite surface.^{5,26} No bands due to O–O stretching were observed these experiments.

4. Discussion

4.1. Photochemistry of Rh(CO)₂/Zeolite—Production of Stable Rhodium Monocarbonyl Surface Species. The ultraviolet photolysis of Rh(CO)₂ species on the surface of zeolite CBV 600 (highly dealuminated zeolite Y) has been investigated. The photochemical decomposition of the zeolite-supported Rh(CO)₂ in a vacuum results in the ejection of a carbonyl ligand

and the production of a stable, coordinatively unsaturated rhodium monocarbonyl surface species, designated $\equiv\text{Rh}(\text{CO})$. It is proposed to coordinate to the surface through the equivalent two chemical bonds. The new, symmetrically line-shaped, infrared band detected at 2023 cm^{-1} (Figure 1) is assigned to the C–O stretching vibration of this monocarbonyl species. To our knowledge, this is the first experimental evidence of this particular species. In the photodecomposition studies of $\text{Rh}(\text{CO})_2$ species supported on Al_2O_3 reported by Wovchko et al.,^{5,6,17} a distinct infrared band was not observed for photochemically produced rhodium monocarbonyl species. A broad, partially overlapped feature near 1975 cm^{-1} was detected; however it was overwhelmed by the strong 2030-cm^{-1} $\text{Rh}(\text{CO})_2$ antisymmetric stretching mode infrared band. Furthermore, photochemically produced, alumina-supported rhodium monocarbonyl species were not stable and were observed to react with surface $\text{Rh}(\text{CO})_2$ to form dinuclear $\text{Rh}_2(\text{CO})_3$ species in the work of Wong and Yates.³ In our work, the new $\equiv\text{Rh}(\text{CO})$ species were stable to 370 K under vacuum. The stability is attributed to the different chemical nature of the zeolite support material surface sites.

This assignment is supported by our isotopic labeling experiments (Figure 2). The ultraviolet photolysis of $\text{Rh}(\text{CO})_2$ and $\text{Rh}(\text{CO})_2$ resulted in the production of $\equiv\text{Rh}(\text{CO})$ and $\equiv\text{Rh}(\text{CO})$ species, displaying infrared bands at 1977 and 1931 cm^{-1} , respectively. The absorption band frequency ratios of $\equiv\text{Rh}(\text{CO})$ to $\equiv\text{Rh}(\text{CO})$ is 0.977, and that of $\equiv\text{Rh}(\text{CO})$ to $\equiv\text{Rh}(\text{CO})$ is 0.954. The experimental frequency ratios are very close to the predicted CO isotopomer ratio values of 0.978 and 0.953, respectively, computed using a simple two-atom reduced mass model. Furthermore, $\text{Rh}(\text{CO})$ species produced photochemically during matrix isolation experiments revealed an infrared spectroscopic band at 2022 cm^{-1} , in excellent agreement with that of the zeolite-supported $\equiv\text{Rh}(\text{CO})$ species.^{30,31} In a recent quantum chemical modeling investigation by Vayssilov et al.,³² an infrared band at 2046 cm^{-1} was calculated, which they assigned to isolated surface rhodium monocarbonyl species on the zeolite surface. This value is in good agreement with our experimentally determined value.

When heating samples containing coordinatively *unsaturated* rhodium monocarbonyl species above 420 K under vacuum, new, coordinatively *saturated* rhodium carbonyl surface species, designated $\equiv\text{Rh}(\text{CO})$, were generated. This saturated species is proposed to coordinate to the surface through the equivalent of three chemical bonds. The infrared band at 2013 cm^{-1} , produced at the expense of the 2023-cm^{-1} band (spectrum b–a, Figure 3), is assigned to saturated $\equiv\text{Rh}(\text{CO})$ species. A band at 2014 cm^{-1} was detected in Miessner's Rh/zeolite carbonyl studies.^{22,23} He attributed this band to a $\text{Rh}(\text{CO})$ surface species but was unable to divulge the nature of its surface coordination. The similar frequencies and reaction conditions in subsequent work allow us to assign Miessner's 2014-cm^{-1} band to the saturated $\equiv\text{Rh}(\text{CO})$. The theoretical work by Vayssilov et al.³² had supported Miessner's rhodium monocarbonyl assignment. However, we believe that there is better frequency agreement between the theoretical rhodium monocarbonyl (2042 cm^{-1}) and our photochemically produced unsaturated $\equiv\text{Rh}(\text{CO})$ species (2023 cm^{-1}). While possible insertion of CO into an Rh–O linkage generates formate-like species, we observed no spectroscopic evidence in the $1550\text{--}1700\text{-cm}^{-1}$ region to support such an assignment.

The photochemical production of $\equiv\text{Rh}(\text{CO})$, and thermal production of $\equiv\text{Rh}(\text{CO})$, is summarized in Scheme 1.

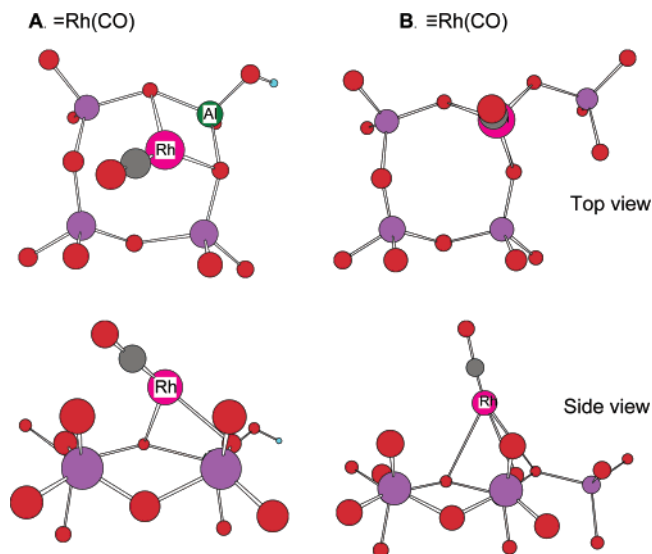
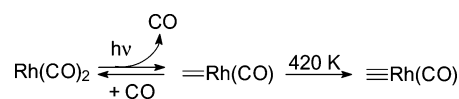


Figure 8. Possible binding structure for $\equiv\text{Rh}(\text{CO})$ (A) and $\equiv\text{Rh}(\text{CO})$ (B) on zeolite T4 and T5 centers, respectively. Redrawn from Figure 6 in ref 33. Atom designations: pink for rhodium, red for oxygen, gray for carbon, and purple for silicon.

SCHEME 1



The coordination site of rhodium on zeolite has been studied by theoretical calculations, EXAFS experiments, infrared, and other spectroscopic methods.^{32–34} $\text{Rh}(\text{CO})_2$ binds with two oxygen centers connected with an aluminum center at a four-ring (T4) of the faujasite network.³⁵ For the unsaturated rhodium monocarbonyl species produced photochemically in this work, it is very likely that this surface binding scheme remains unchanged after one CO ligand is lost from the rhodium center. Upon heating, the thermal energy supplied to the sample assists the unsaturated rhodium monocarbonyl species to extend its surface coordination by migrating to a nearby T5 center. There, three bonds between the rhodium center and three oxygen atoms are formed. The proposed binding sites for both $\equiv\text{Rh}(\text{CO})$ and $\equiv\text{Rh}(\text{CO})$ are shown schematically in Figure 8. The proposed unusual structure is possible by the geometry constraints imposed by the zeolite framework.³⁶ Although the energy of the saturated monocarbonyl structure is high, there may be no easy way to reconfigure by coordination of an incoming ligand because of a high energy barrier. Since no $\text{Rh}_2(\text{CO})_3$ were detected during our experiments, the migration of $\equiv\text{Rh}(\text{CO})$ to nearby $\text{Rh}(\text{CO})_2$ does not occur on 0.5% Rh/zeolite samples up to 420 K. Assuming complete dispersion of Rh on the zeolite surface, there is one Rh atom per 10 supercages on average for the samples used in this work.³⁸ The relatively long distance of 52 Å between Rh centers also inhibits $\text{Rh}_2(\text{CO})_3$ formation.

4.2. Reaction of Coordinatively Unsaturated Rhodium Monocarbonyl Species with N_2 , H_2 , and O_2 Gas Molecules.

We consider the new $\equiv\text{Rh}(\text{CO})$ surface species to be coordinatively unsaturated on the basis of its chemical reactivity to various gas phase molecules. Though not presented spectroscopically in Results, $\equiv\text{Rh}(\text{CO})$ promptly captures a CO molecule to regenerate $\text{Rh}(\text{CO})_2$ when exposed to CO gas at room temperature. Furthermore, N_2 , H_2 and O_2 gas molecules react readily with $\equiv\text{Rh}(\text{CO})$ surface species. Infrared spectroscopic evidence is presented in Figures 4–7. During each experiment, the 2023-cm^{-1} infrared band due to $\equiv\text{Rh}(\text{CO})$

SCHEME 2



species decreases, while new bands develop in other regions of the infrared spectrum. The developing bands were due to the formation of new surface species.

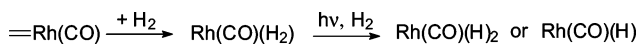
The reaction of =Rh(CO) with N₂ at room temperature led to the formation of Rh(CO)(N₂) surface species. The vacant coordination site on the Rh center readily accepts the σ -orbital electron donation from the N₂ ligand. The infrared band at 2252 cm⁻¹ (Figure 4) is assigned to the N₂ stretching vibration of the surface rhodium dinitrogen carbonyl complex. The infrared band at 2062 cm⁻¹ is due to the CO stretching vibration of Rh(CO)(N₂). These modes appropriately shifted or remained unchanged in isotopic labeling experiments (Table 1). Similar species were generated photochemically on Rh/Al₂O₃ samples at 175 K, with respective infrared bands at 2234 and 2048 cm⁻¹.^{5,39} Miessner detected Rh(CO)(N₂) species formation during high-temperature (523 K) and high-pressure flow experiments on Rh/zeolite, with very similar infrared bands appearing at 2251 and 2060 cm⁻¹.^{22,23} The N₂ ligand presumably coordinates to the Rh center in an η^1 -end-on configuration as in the Rh/Al₂O₃ work.^{5,39} The N₂ reaction with =Rh(CO) species is summarized in Scheme 2.

The reaction with N₂ gas was reversible. Upon evacuation of the N₂ gas at room temperature, Rh(CO)(N₂) species slowly lose N₂ ligands to regenerate =Rh(CO) species. The loss of the 2252- and 2062-cm⁻¹ Rh(CO)(N₂) features and gain of the 2023-cm⁻¹ =Rh(CO) feature in Figure 4 indicate this. Reintroduction of N₂ gas causes Rh(CO)(N₂) to re-form. Heating a sample with Rh(CO)(N₂) species above 370 K results in the formation of saturated =Rh(CO).

The decision to label the =Rh(CO) species produced during thermal decomposition experiments in Figures 3 and 4 as coordinatively saturated is logical, since the species are unreactive to N₂ gas. This is evident since no significant intensity change occurs with the 2013-cm⁻¹ infrared band during evacuation and reintroduction of N₂ gas (Figure 4). This differs from the observation of obvious spectroscopic changes for the highly active unsaturated =Rh(CO) species when reacting with N₂ and other gas molecules.

To further explore the chemical reactivity of the unsaturated rhodium monocarbonyl surface species, we conducted a room-temperature reaction of =Rh(CO) with H₂ gas molecules (Figure 5). The overlapping infrared bands detected at 2096 and 2092 cm⁻¹ are assigned to the CO stretching vibrations of surface Rh(CO)(H₂) species. After an unsaturated =Rh(CO) species captures an H₂ molecule, the H–H bond of the H₂ ligand is proposed to remain unbroken or partially activated. H₂ most likely coordinates with a Rh center in a η^2 -side-on fashion, as with Rh/Al₂O₃,^{5,6} since no infrared bands appear near 4161 cm⁻¹ due to H–H stretching.^{40,41} By irradiating Rh(CO)(H₂) species at room temperature in the presence of H₂ gas, the H–H bond is broken, and Rh(CO)(H₂) or Rh(CO)(H) species are generated. It is conceivable that a photochemical reaction between Rh(CO)₂ and H₂ occurs; however, very little change was observed in the intensity of the Rh(CO)₂ infrared bands (Figure 5). The infrared band detected at 2102 cm⁻¹ is assigned to the CO stretching vibration of Rh(CO)(H₂) or Rh(CO)(H) species. The H₂ reaction with =Rh(CO) is illustrated in Scheme 3.

SCHEME 3

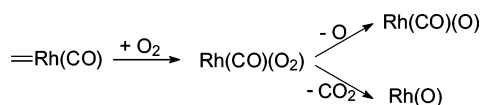


Rhodium carbonylhydrido surface species can also be made during elevated temperature (420 K) hydrogen gas reduction of Rh(CO)₂ surface species. Miessner²³ reported an infrared band at 2093 cm⁻¹ due to a rhodium monocarbonyl species. Vayssilov reevaluated this assignment and found it to be incorrect.³² Instead of rhodium monocarbonyl species, Rh(CO)(H₂) or H–H partially dissociated species Rh(CO)(H)₂ were assigned to this band. Our decision to assign the 2102-, 2096-, and 2092-cm⁻¹ bands to Rh(CO)(H₂), Rh(CO)(H), and/or Rh(CO)(H₂) is based on a comparison with similar experimental and theoretical results reported for H₂ reactions with heterogeneous phase rhodium carbonyl surface species^{42–45} and homogeneous phase rhodium carbonyl complexes.^{32,46–51} The possibility that this set of bands is due to Rh–H stretching vibrations has been eliminated on the basis of our =Rh(CO) reaction with D₂ gas. Bands in the CO stretching region during the D₂ experiment were still observed, but no band near 1440 cm⁻¹ was detected (Figure 6). Furthermore, during a H₂ reaction with isotopically labeled rhodium carbonyl species, appropriate shifts of the new carbonyl bands occurred. The slight shifts of the carbonyl bands to 2101 and 2098 cm⁻¹ in the D₂ reaction indicates the influence of the D atom coupled to CO oscillation frequency for the Rh(CO)-(D)₂ or Rh(CO)(D) species. In both H₂ and D₂ experiments, we did not detect Rh–H or Rh–D infrared spectroscopic bands and assume that their absorption coefficients are small. In the D₂ experiment, breakage of the D–D bond and D-atom spillover onto the zeolite support did occur since deuterated surface hydroxyl groups formed.

The unsaturated rhodium monocarbonyl surface species reacted with O₂ gas at 302 and 340 K (Figure 7). Again, an immediate loss of the 2023-cm⁻¹ =Rh(CO) infrared band occurred after introducing O₂ into the cell. After 3 min at 302 K (Figure 7A), a new band appeared at 2130 cm⁻¹ and is assigned to the CO stretching vibration of oxidized rhodium carbonyl surface species, designated Rh(CO)(O). The band shifted to 2083 cm⁻¹ in Rh(¹³CO)(O) when ¹³CO-labeled sample was used. (Spectra were not shown.) A similar infrared band was reported for analogous oxidized rhodium carbonyl species found on Rh/Al₂O₃.^{5,7} Since no infrared spectroscopic features were observed for O–O stretching vibrations, it is apparent that the O–O bond of the coordinated O₂ ligand is broken. By conducting the reaction at 340 K (Figure 7B), it becomes clear that an oxygen atom from O₂ migrates to the CO ligand to generate CO₂. The production of CO₂ gas was confirmed with isotopic substitution experiments.

The reaction of O₂ with =Rh(CO) was not reversible, as was the reaction of =Rh(CO) with N₂. The 2130-cm⁻¹ Rh(CO)(O) infrared band decreased in intensity during thermal evacuation at 302 K (data not shown). However, no new infrared band at 2023 cm⁻¹ appeared to indicate regeneration of unsaturated rhodium monocarbonyl species. The N≡N bond in N₂ was not activated like the O=O bond in O₂. Furthermore, Rh(CO)₂ surface species were produced during the O₂ reaction with unsaturated rhodium monocarbonyl species. Evidence for this is the development of infrared bands at 2118 and 2053 cm⁻¹. The formation of Rh(CO)₂ can be explained by a proposed alternative reaction in which the CO ligand is lost from Rh(CO)(O) to generate CO gas and surface rhodium oxo species of the form Rh(O). Rhodium oxo species have been reported in the heterogeneous phase^{52–54} and in the homogeneous phase.^{55–57} We were unable to detect low-frequency Rh=O

SCHEME 4



infrared bands near 800 cm^{-1} , due to the strongly absorbing lattice vibrations of the zeolite below 1000 cm^{-1} . Before diffusion outside of the porous zeolite material, the CO ligand was captured by another surface rhodium monocarbonyl species to produce surface Rh(CO)_2 . The =Rh(CO) reaction with O_2 is summarized in Scheme 4.

5. Conclusions

Well-defined rhodium dicarbonyl species supported on dealuminated zeolite Y is a good starting material for the photochemical production of stable, but active, new coordinatively unsaturated rhodium monocarbonyl species. The unsaturated rhodium monocarbonyl species react with N_2 , H_2 , and O_2 gas molecules at room temperature. The following conclusions have been reached.

(1) A new coordinatively unsaturated rhodium monocarbonyl species, =Rh(CO) , has been prepared for the first time on the surface of zeolite Y (CBV600) by the $350 \pm 50\text{ nm}$ ultraviolet photolysis of supported Rh(CO)_2 . The =Rh(CO) species were stable to 370 K under vacuum. An infrared band at 2023 cm^{-1} was assigned to it.

(2) Coordinatively saturated rhodium monocarbonyl species, =Rh(CO) , were produced by heating a sample with photochemically generated =Rh(CO) species above 370 K in a vacuum. Saturated rhodium monocarbonyl surface species were stabilized through extended coordination with the zeolite surface and did not react with N_2 gas. This saturated monocarbonyl species has a characteristic infrared band at 2013 cm^{-1} .

(3) Unsaturated rhodium monocarbonyl species rapidly, and reversibly, coordinate N_2 gas molecules to form $\text{Rh(CO)(N}_2\text{)}$ surface species. Infrared bands were detected at 2252 cm^{-1} for the $\text{N}\equiv\text{N}$ stretching mode and 2062 cm^{-1} for the carbonyl stretching vibration of the $\text{Rh(CO)(N}_2\text{)}$ surface complex.

(4) =Rh(CO) species capture H_2 gas molecules to form $\text{Rh(CO)(H}_2\text{)}$ species on the zeolite surface. The H-H bond in $\text{Rh(CO)(H}_2\text{)}$ can be broken by UV irradiation to produce Rh(CO)(H) and/or Rh(CO)(H) . Carbon dioxide and a proposed surface rhodium oxo species of the form Rh(O) are produced from the reaction of =Rh(CO) species with O_2 gas.

(5) The work provides new insight into the photochemical behavior of Rh(CO)_2 species supported on high area zeolite materials and may improve our understanding of the role of active rhodium monocarbonyl species in the development of heterogeneous photocatalysts.

Acknowledgment. We acknowledge financial support from Bryn Mawr College. We thank Zeolyst for supplying zeolite samples.

References and Notes

- (1) Ballinger, T. H.; Yates, J. T., Jr. *J. Am. Chem. Soc.* **1992**, *114*, 10074.
- (2) Ballinger, T. H.; Yates, J. T., Jr. *J. Phys. Chem.* **1992**, *96*, 9979.
- (3) Wong, J. C. S.; Yates, J. T., Jr. *J. Am. Chem. Soc.* **1994**, *116*, 1610.
- (4) Wong, J. C. S.; Yates, J. T., Jr. *J. Phys. Chem.* **1995**, *99*, 12640.
- (5) Wovchko, E. A.; Yates, J. T., Jr. *Langmuir* **1999**, *15*, 3506.
- (6) Wovchko, E. A.; Yates, J. T., Jr. *J. Am. Chem. Soc.* **1995**, *117*, 12557.
- (7) Wovchko, E. A.; Yates, J. T., Jr. *J. Am. Chem. Soc.* **1998**, *120*, 10523.
- (8) Wovchko, E. A.; Yates, J. T., Jr. *J. Am. Chem. Soc.* **1998**, *120*, 7544.
- (9) Dougherty, T. P.; Grubbs, W. T.; Heilweil, E. J. *J. Phys. Chem.* **1994**, *98*, 9396.
- (10) Yang, H.; Kotz, K. T.; Asplund, M. C.; Wilkens, M. J.; Harris, C. B. *Acc. Chem. Res.* **1999**, *32*, 551.
- (11) Bengali, A. A.; Schultz, R. H.; Moore, C. B.; Bergman, R. G. *J. Am. Chem. Soc.* **1994**, *116*, 9585.
- (12) Rest, A. J.; Whitwell, I.; Graham, W. A. G.; Hoyano, J. K.; McMaster, A. D. *J. Chem. Soc., Chem. Commun.* **1984**, 624.
- (13) Rest, A. J.; Whitwell, I.; Graham, W. A. G.; Hoyano, J. K.; McMaster, A. D. *J. Chem. Soc., Dalton Trans.* **1987**, 1181.
- (14) Dunwoody, N.; Sun, S.-S.; Lees, A. J. *Inorg. Chem.* **2000**, *39*, 4442.
- (15) Lees, A. J. *J. Organomet. Chem.* **1998**, *554*, 1–11.
- (16) Crabtree, R. H. *Chem. Rev.* **1995**, *95*, 987.
- (17) Wovchko, E. A.; Zubkov, T. S.; Yates, J. T., Jr. *J. Phys. Chem. B* **1998**, *102*, 10535.
- (18) Asbury, J. B.; Ghosh, H. N.; Yeston, J. S.; Bergman, R. G.; Lian, T. *Organometallics* **1998**, *17*, 3417.
- (19) Jacobs, P. A. *Zeolite Chemistry and Catalysis*; Elsevier: New York, 1991.
- (20) Jansen, J. C. *Advanced Zeolite Science and Applications*; Elsevier: New York, 1994.
- (21) Miessner, H.; Burkhardt, I.; Gutschick, D.; Zecchina, A.; Morterra, C.; Spoto, G. *J. Chem. Soc., Faraday Trans. 1* **1989**, *85*, 2113.
- (22) Miessner, H. *J. Chem. Soc., Chem. Commun.* **1994**, 927.
- (23) Miessner, H. *J. Am. Chem. Soc.* **1994**, *116*, 11522.
- (24) Basu, P.; Ballinger, T. H.; Yates, J. T., Jr. *Rev. Sci. Instrum.* **1988**, *59*, 1321.
- (25) Wang, X.; Wovchko, E. A. Manuscript in preparation.
- (26) Yates, J. T., Jr.; Duncan, T. M.; Vaughan, R. W. *J. Chem. Phys.* **1979**, *71*, 3908.
- (27) Wang, X.; Andrews, L. *J. Phys. Chem. A* **2002**, *106*, 3706.
- (28) Hair, M. L. *Infrared Spectroscopy in Surface Chemistry*; Marcel Dekker: New York, 1967.
- (29) Shimanouchi, T. *Molecular Vibrational Frequencies*. In *NIST Chemistry WebBook, NIST Standard Reference Database Number 69*, Linstrom, P. J.; Mallard, W. G., Eds.; National Institute of Standards and Technology: Gaithersburg, MD, 2003.
- (30) Zhou, M.; Andrews, L. *J. Am. Chem. Soc.* **1999**, *121*, 9171.
- (31) Zhou, M.; Andrews, L. *J. Phys. Chem. A* **1999**, *103*, 7773.
- (32) Vayssilov, G. N.; Rösch, N. *J. Am. Chem. Soc.* **2002**, *124*, 3783.
- (33) Goellner, J. F.; Gates, B. C.; Vayssilov, G. N.; Rösch, N. *J. Am. Chem. Soc.* **2000**, *122*, 8056.
- (34) Molitor, P. F.; Shoemaker, R. K.; Apple, T. M. *J. Phys. Chem.* **1989**, *93*, 3, 2891.
- (35) Webber, W. A. Ph. D. Dissertation, University of California, Davis, 1998.
- (36) A distorted tetrahedral structure is proposed for the saturated =Rh(CO) species. This is different from a square planar coordination structure adopted by surface Rh(CO)_2 species and helps to explain its greater stability gained from the additional coordination, compared to the 3-coordinate, unsaturated rhodium monocarbonyl. While purely tetrahedral geometries are not prevalent in d^8 metal complexes, some examples have been reported, such as $[\text{NiCl}_4]^{2-}$, $[\text{Rh(PMe}_3)_4]^+$, and $\text{CoBr(PR}_3)_3$.³⁷ It is expected that the usual degeneracy of the d-based molecular orbitals in a tetrahedral configuration is lost as a result of the nonequivalence of the CO ligand and the three surface oxide coordination sites. This may help stabilize a d^8 Rh center.
- (37) Cotton, F. A.; Wilkinson, G. *Advanced Inorganic Chemistry*, 5th ed.; John Wiley & Sons: New York, 1988; pp 725, 742, 902.
- (38) This value was estimated on the basis of the supercage density of zeolite Y, 5.56×10^{20} per 2 g of sample. The cell parameters are $a = b = c = 24.345\text{ Å}$. See http://www.zeolites.ethz.ch/Zeolites/FMPPro?-db=Atlas_main.fp5&-lay=web%20layout&-format=FWtopology.htm&STC=FAU&-find. Access date, July 01, 2003.
- (39) Wovchko, E. A.; Yates, J. T., Jr. *J. Am. Chem. Soc.* **1996**, *118*, 10250.
- (40) Nakamoto, K. *Infrared Spectra of Inorganic and Coordination Compounds*; Wiley: New York, 1963.
- (41) Herzberg, G. *Molecular Spectra and Molecular Spectroscopy I: Spectra of Diatomic Molecules*, 2nd ed.; Van Nostrand Reinhold: New York, 1979.
- (42) Mukhopadhyay, K.; Mandale, A. B.; Chaudhari, R. V. *Chem. Mater.* **2003**, *15*, 1766.
- (43) Park, S. C.; Ekerdt, J. G. *J. Mol. Catal.* **1984**, *24*, 33.
- (44) Henderson, M. A.; Worley, S. D. *J. Phys. Chem.* **1985**, *89*, 1417.
- (45) Hayden, B. E.; King, A.; Newton, M. A. *Surf. Sci.* **1998**, *397*, 306.
- (46) Nozaki, K.; Matsuo, T.; Shibahara, F.; Hiyama, T. *Organomet.* **2003**, *22*, 594.
- (47) Aghmiz, A.; Orejon, A.; Dieguez, M.; Miquel-Serrano, M. D.; Claver, C.; Masdeu-Butto, A. M.; Sinow, D.; Laurencsy, G. *J. Mol. Catal. A: Chem.* **2003**, *195*, 113.

- (48) Kingston, D. G.; Kolpak, M. X. *J. Am. Chem. Soc.* **1980**, *102*, 5966.
- (49) Yoshida, T.; Okano, T.; Ueda, Y.; Otsuka, S. *J. Am. Chem. Soc.* **1981**, *103*, 3411.
- (50) Balch, A. L.; Lee, J. W.; Noll, B. C.; Olmstead, M. M. *Inorg. Chem.* **1993**, *32*, 3577.
- (51) Taw, F. L.; Mellows, H.; White, P. S.; Hollander, F. J.; Bergman, R. G.; Brookhart, M.; Heinekey, D. M. *J. Am. Chem. Soc.* **2002**, *124*, 5100.
- (52) Rice, C. A.; Worley, S. D.; Curtis, C. W.; Guin, J. A.; Tarrer, A. R. *J. Chem. Phys.* **1981**, *74*, 6487.
- (53) Wey, J. P.; Neely, W. C.; Worley, S. D. *J. Catal.* **1992**, *134*, 378.
- (54) Citra, A.; Andrews, L. *J. Phys. Chem. A* **1999**, *103*, 4845.
- (55) Aresta, M.; Tommasi, I.; Quaranta, E.; Fragale, C.; Mascetti, J.; Tranquille, M.; Galan, F.; Fouassier, M. *Inorg. Chem.* **1996**, *35*, 4254.
- (56) McGinnety, J. A.; Payne, N. C.; Ibers, J. A. *J. Am. Chem. Soc.* **1969**, *91*, 6301.
- (57) Ho, D. G.; Ismail, R.; Franco, N.; Gao, R.; Leverich, E. P.; Tsyba, I.; Ho, N. N.; Bau, R.; Selke, M. *Chem. Commun.* **2002**, 570.